AMSE JOURNALS-AMSE IIETA publication-2017-Series: Modelling B; Vol. 86; N°3; pp 782-807
Submitted Apr. 13, 2017; Revised Jan. 04, 2018; Accepted Jan. 11, 2018
https://doi.org/10.18280/mmc_b.860311

Slip Effects on MHD Flow of a Williamson Fluid from an Isothermal Sphere: A Numerical Study

N. Nagendra, C.H. Amanulla., M. Sudhakar Reddy

Department of Mathematics, Madanapalle Institute of Technology and Science, Madanapalle-517325, India. (nagsvu76@gmail.com)

Abstract

In the present paper, we investigated mathematical model of the magneto hydrodynamic flow and heat transfer in an electro-conductive polymer on the external surface of a sphere under radial magnetic field is presented. Thermal and velocity (hydrodynamic) slip are considered at the sphere surface via. modified boundary conditions. The non-dimensional, transformed boundary layer equations for momentum and energy are solved with the second order accurate implicit Keller box finite difference method under appropriate boundary conditions. Validation of the numerical solutions is achieved via benchmarking with earlier published results. The influence of Weissenberg number, magnetic body force parameter, thermal slip parameter, hydrodynamic slip parameter, stream wise variable and Prandtl number on thermo fluid characteristics are studied graphically and via tables. A weak elevation in temperature accompanies increasing Weissenberg number whereas a significant acceleration in the flow is computed near the sphere surface with increasing Weissenberg number. Increasing thermal slip strongly decreases skin friction and Nusselt number. Skin friction is also depressed with increasing magnetic body force parameter. Increasing momentum slip is observed to decrease skin friction. Nusselt number is reduced with increasing Weissenberg number. Skin friction is increased whereas Nusselt number is reduced with greater stream wise coordinate. The study is relevant to smart coating transport phenomena.

Key words

Weissenberg number, Williamson model, magneto hydrodynamics, Thermal convection, non-Newtonian flow, boundary layers, thermal and momentum slip.

1. Introduction

Magnetohydrodynamic has found ever-increasing applications in modern smart technologies. The application of magnetic fields (static or alternating) has been shown to manipulate successfully the material characteristics of electro-conductive polymers which are finding new applications in aerospace, offshore and naval industries. Interesting studies in this regard addressing various systems employing magnetic polymers include environmental engineering [1], thin film fabrication processes [2] and design of shock dissipation systems with magnetic elastomers [3]. Coating applications and energy systems enhancement with smart magnetic polymers have also grown substantially in recent years. Relevant technologies in this regard are nuclear engineering [4], medical engineering exploiting stimuli-based polymers [5] and hydromagnetic energy generation [6]. In the context of coating applications, it is critical to regulate heat transfer conditions which lead to improved bonding and homogeneity in engineered polymeric surfaces. Many studies have therefore examined the transport phenomena (i.e. coupled heat and momentum transfer) from different geometrical shapes including cones, pipes, disks and truncated bodies and spheres. The spherical geometry is particularly relevant to chemical engineering processes. Investigators have applied a variety of different material models for the coatings and also numerical methods to solve the associated boundary value problems. Bég et al. [7] used the Homotopy analysis method (HAM) to analyze flow from a sphere in a porous medium. Musong and Feng [8] used an immersed boundary method algorithm to simulate the mixed thermal convection from a heated sphere for an arbitrary flow incident angle over a range of Reynolds numbers and Richardson numbers considering both aiding and cross flow and opposed flow. Juncu [9] utilized a splitting finite difference code to study computationally the transient, dissipative conjugate, forced convection heat transfer from a sphere to a surrounding fluid flow, considering the influence of Brinkman and Peclet numbers on heat transfer rates.

The above studies were confined to Newtonian fluids. However, generally polymers are known to exhibit non-Newtonian characteristics. Engineers have developed a variety of constitutive models to analyze the shear stress-strain characteristics of these fluids, including viscoplastic, viscoelastic, micro-structural and power-law models. Both purely fluid flow and heat transfer from a sphere to non-Newtonian fluids have been reported in a number of theoretical investigations. Verma [10] presented analytical solutions for viscoelastic boundary layer flow of revolution (sphere), noting that there is a displacement in the point of separation of the boundary layer with increasing elasticity effect. Cheng [11] investigated free convection heat and mass transfer from a sphere in micropolar fluids with isosolutal and isothermal boundary conditions. Amanulla et al. [12] investigated slip effects on Casson Nano fluid flow from an isothermal

sphere. They analyzed the behavior of a fluid on velocity and temperature distributions when thermal and velocity slips are considered. Dasman et al. [13] employed the Walters-B Non-Newtonian model to study free and forced convection flow from a sphere. Dasman [14] considered heat transfer in external boundary layer flows from a sphere for a variety of viscoelastic fluids. Bhatnagar [15] presented analytical solutions for thermal convection in elastic-viscous flow from a spinning, insulated sphere, correlating his findings with experiments on polysiloxane, and observing that the secondary flow breaks down into two regimes wherein heat convection dominates dissipation effects due to viscoelasticity of the polymer. These studies however did not consider the Williamson model. This is a shear-thinning non-Newtonian model which quite accurately simulates polymer viscoelastic flows over a wide spectrum of shear rates. In Williamson fluids the viscosity is reduced with rising shear stress rates. This model has found some popularity in engineering simulations. Maboob et al. [16] used the Quasi-linearization technique to analyze Magnetohydrodynamic radiative flow of Williamson viscoelastic nanofluid from a heated surface. Khan and Khan [17] investigated Blasius, Sakiadis, stretching and stagnation point flows of Williamson fluid using the Homotopy analysis method, over a range of Weissenberg numbers. Bég et al. [18] presented extensive numerical solutions for hydromagnetic pumping of a Williamson fluid using a modified differential transform method, observing that a change in Weissenberg number strongly modifies the pressure difference and axial velocity. Further studies of transport phenomena in Williamson fluids include Rao and Rao [19] and Dapra and Scarpi [20].

In the present investigation, admitted the Magneto hydrodynamic convection boundary layer flow of a Williamson polymeric fluid external to a stationary solid sphere with multiple slip effects. Magnetic fields have been found to profoundly influence heat transfer and velocity characteristics in curved body flows. Relevant examples include Bég et al. [21] (for cylindrical geometries), Alkasasbeh et al. [22] who addressed radiative effects also, Amanulla et al. [23] who considered partial slip effects and Kasim et al. [24] who used a viscoelastic model. Slip effects have been shown to be prominent in certain polymeric flow processes. Momentum (hydrodynamic) slip relates to the non-adherence of the polymer to a solid boundary and arises in polymer melts, emulsions, petro-chemical suspensions and also foams [25-33]. The presence of momentum slip invalidates the classical “no-slip” boundary condition. Thermal slip may also arise in heat transfer problems and can also significantly modify both velocity and temperature characteristics both at the solid surface and deeper into the boundary layer. Several researchers have examined multi-physical flows with velocity and/or thermal slip effects including Jamil and Khan [34], Tripathi et al. [35] (for viscoelastic fluids), Bég et al. [36] for Magnetohydrodynamic

heat and mass transfer and Devi and Devi [37] for swirling disk hydromagnetic flows with cross diffusion. Amanulla et al. [37] have studied numerically the slip effects in MHD flow and heat transfer of Williamson fluids over a truncated cone. The present study employs a finite difference numerical method due to Keller for solving the two-dimensional steady slip flow and heat transfer in a Williamson polymeric liquid boundary layer from a sphere. Verification of the computations is conducted for the special case of non-magnetic, Newtonian flow in the absence of slip with earlier published literature. The study finds applications in electro-conductive thermal polymer processing systems.

2. Mathematical Model

The regime under investigation is illustrated in **Fig. 1**. Steady, incompressible hydromagnetic Williamson non-Newtonian boundary layer flow and heat transfer from a spherical body under radial magnetic field is considered.

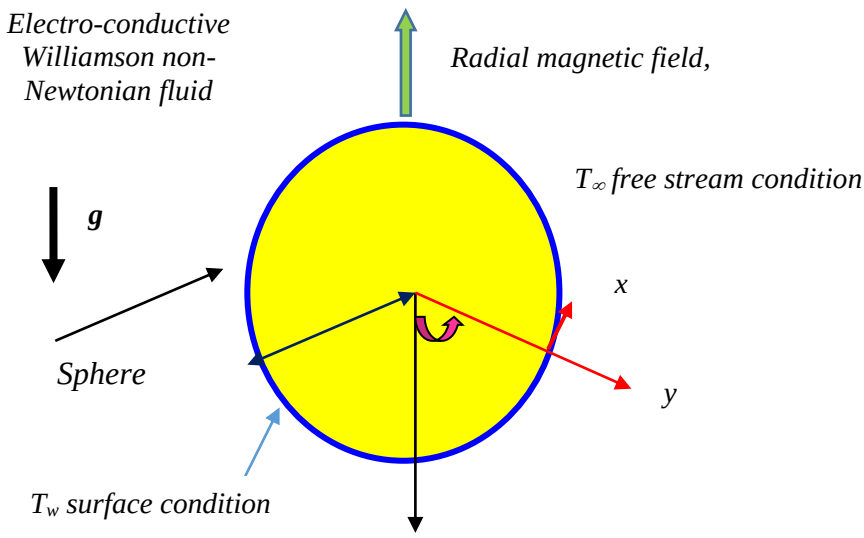

Fig 1. Magnetohydrodynamic non-Newtonian heat transfer

For an incompressible Williamson fluid, the continuity (mass conservation) and momentum equations are given as:

$$\mathrm{div}\ V = 0, \tag{1}$$

$$\rho \frac{dV}{dt} = \mathrm{div} S + \rho b, \tag{2}$$

Where ρ is the density of the fluid, V is the velocity vector, S is the Cauchy stress tensor, *b* represents the specific body force vector, and d/dt represents the material time derivate. The constitutive equations of the Williamson fluid model [16-20] are given as:

$$S = -pI + \tau \tag{3}$$

$$\tau = \left[\mu_\infty + \frac{(\mu_0 - \mu_\infty)}{1 - \Gamma\dot{\gamma}} \right] A_1, \tag{4}$$

Here p is the pressure, I is the identity vector, τ is the extra stress tensor, μ_0, μ_∞ are the limiting viscosities at zero and at infinite shear rate, Γ is the time constant (>0), A_1 is the first Rivlin-Erickson tensor and $\dot{\gamma}$ is defined as follows:

$$\dot{\gamma} = \sqrt{\frac{1}{2}\pi}, \tag{5}$$

$$\pi = trace(A_1^2) \tag{6}$$

Here considered the case for which $\mu_\infty = 0$ and $\Gamma\dot{\gamma} < 1.$ Thus eq. (4) can be written as:

$$\tau = \left(\frac{\mu_0}{1 - \Gamma\dot{\gamma}} \right) A_1, \tag{7}$$

By using binomial expansion, we get:

$$\tau = \mu_0 \left[1 + \Gamma\dot{\gamma} \right] A_1. \tag{8}$$

The two-dimensional mass, momentum and energy boundary layer equations governing the flow in an (*x*,*y*) coordinate system may be shown to take the form:

$$\frac{\partial(ru)}{\partial x} + \frac{\partial(rv)}{\partial y} = 0 \tag{9}$$

$$u\frac{\partial u}{\partial x} + v\frac{\partial u}{\partial y} = \nu\frac{\partial^2 u}{\partial y^2} + \sqrt{2}\nu\Gamma\frac{\partial u}{\partial y}\frac{\partial^2 u}{\partial y^2} + g\beta(T - T_\infty)\sin\left(\frac{x}{a}\right) - \frac{\sigma B_0^2}{\rho}u \tag{10}$$

$$u\frac{\partial T}{\partial x} + v\frac{\partial T}{\partial y} = \alpha\frac{\partial^2 T}{\partial y^2} \tag{11}$$

The boundary conditions for the considered flow with velocity and thermal slip are:

$$\text{At } y=0, \quad u=N_0\frac{\partial u}{\partial y},\ v=0,\ T=T_w+K_0\frac{\partial T}{\partial y}$$

$$\text{As } y\to\infty,\ u\to 0,\ v\to 0,\ T\to T_\infty \tag{12}$$

Here N_0 is the velocity slip factor, K_0 is the thermal slip factor and T_∞ is the free stream temperature. For $N_0=0=K_0$, one can recover the no-slip case. The stream function ψ is defined by $ru=\frac{\partial(r\psi)}{\partial y}$ and $rv=-\frac{\partial(r\psi)}{\partial x}$, and therefore, the continuity equation is automatically satisfied. In order to write the governing equations and the boundary conditions in dimensionless form, the following non-dimensional quantities are introduced:

$$\xi=\frac{x}{a},\ \eta=\frac{y}{a}Gr^{1/4},\ f(\xi,\eta)=\frac{\psi}{\nu\xi Gr^{1/4}},\ \theta(\xi,\eta)=\frac{T-T_\infty}{T_w-T_\infty}$$

$$\Pr=\frac{\nu}{\alpha},Gr=\frac{g\beta(T_w-T_\infty)a^3}{\nu^3},We=\frac{\sqrt{2}\,\nu\Gamma\,xGr^{3/4}}{a^3} \tag{13}$$

The emerging momentum and heat (energy) conservation equations in dimensionless from assume the following form:

$$f'''+(1+\xi\cot\xi)ff''-f'^2+Wef''f'''+\frac{\sin\xi}{\xi}\theta-Mf'=\xi\left(f'\frac{\partial f'}{\partial\xi}-f''\frac{\partial f}{\partial\xi}\right) \tag{14}$$

$$\frac{\theta''}{\Pr}+(1+\xi\cot\xi)f\theta'=\xi\left(f'\frac{\partial\theta}{\partial\xi}-\theta'\frac{\partial f}{\partial\xi}\right) \tag{15}$$

The transformed dimensionless boundary conditions are reduced to:

$$\text{At } \eta=0,\ f=0,\ f'=S_f f''(0),\ \theta=1+S_T\theta'(0)$$

$$\text{As } \eta\to\infty,\ f'\to 0,\ \theta\to 0 \tag{16}$$

The skin-friction coefficient (sphere surface shear stress) and the local Nusselt number (sphere surface heat transfer rate) can be defined, respectively, using the transformations described above with the following expressions:

$$Gr^{-3/4}C_f = \xi f''(\xi,0) + \frac{We}{2}\xi(f''(\xi,0))^2 \tag{17}$$

$$Gr^{-1/4}Nu = -\theta'(\xi,0) \tag{18}$$

All parameters are defined in the nomenclature.

3. Computational Solution with Keller Box Implicit Method

The transformed, nonlinear, multi-physical boundary value problem defined by Eqns. (14)-(16) can be solved via. a number of numerical schemes. Here we implement a popular, second order accurate implicit finite difference method originally developed by Keller [39]. Recent studies featuring this method in the context of magnetohydrodynamic and rheological flows include Sajid *et al*. [40] who studied ferrofluid flows in curved conduits, Amanulla *et al*. [41] who investigated hydromagnetic non-Newtonian convection from a cone and convective Williamson boundary layer flows by Amanulla *et al.* [42]. In the Keller box scheme, the multi-degree, multi-order coupled partial differential equations defined in (14) and (15) are first reduced to a system of first order equations. These equations are then discretized with the finite difference approximations with appropriate step lengths in each coordinate direction. Introducing the new variables:

$$u(x,y) = f', v(x,y) = f'', s(x,y) = \theta \tag{19}$$

$$f' = u \tag{20}$$

$$u' = v \tag{21}$$

$$\theta' = t \tag{22}$$

Eqns. (14)-(15) reduce then to the form:

$$v' + (1+\xi\cot\xi)fv + Wevv' - u^2 + \frac{\sin\xi}{\xi}s - Mu = \xi\left(u\frac{\partial u}{\partial\xi} - v\frac{\partial f}{\partial\xi}\right) \tag{23}$$

$$\frac{t'}{\Pr} + (1+\xi\cot\xi)ft = \xi\left(u\frac{\partial s}{\partial\xi} - t\frac{\partial f}{\partial\xi}\right) \tag{24}$$

where primes denote differentiation with respect to η . In terms of the dependent variables, the boundary conditions (16) become:

At $\eta = 0,\ f = 0,\ f' = S_f\, f''(0), \theta = 1 + S_T \theta'(0)$

As $\eta \to \infty,\ f' \to 0,\ \theta \to 0$ (25)

A two-dimensional computational mesh (grid) is imposed on the ξ-η plane as shown in **Fig.2**. The stepping process is defined by:

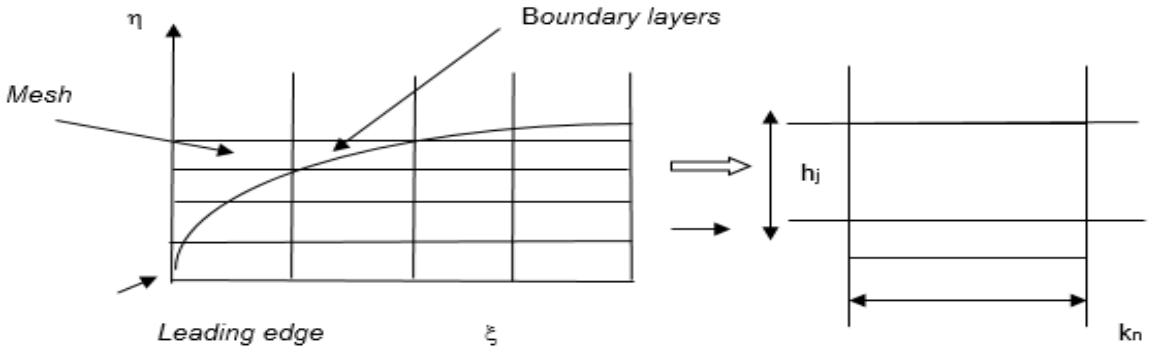

Fig. 2 Keller Box element and boundary layer mesh

where k_n and h_j denote the step distances in the ξ and η directions respectively.

$$\eta_0 = 0,\ \eta_j = \eta_{j-1} + h_j,\ j = 1, 2, ..., J,\ \eta_J \equiv \eta_\infty \tag{26}$$

$$\xi^0 = 0,\ \xi^n = \xi^{n-1} + k_n,\ n = 1, 2, ..., N \tag{27}$$

If g_j^n denotes the value of any variable at $\left(\eta_j, \xi^n\right)$, then the variables and derivatives of Equations. (20) – (24) at $\left(\eta_{j-1/2}, \xi^{n-1/2}\right)$ are replaced by:

$$g_{j-1/2}^{n-1/2} = \frac{1}{4}\left(g_j^n + g_{j-1}^n + g_j^{n-1} + g_{j-1}^{n-1}\right), \tag{28}$$

$$\left(\frac{\partial g}{\partial \eta}\right)_{j-1/2}^{n-1/2} = \frac{1}{2h_j}\left(g_j^n - g_{j-1}^n + g_j^{n-1} - g_{j-1}^{n-1}\right), \tag{29}$$

$$\left(\frac{\partial g}{\partial \xi}\right)_{j-1/2}^{n-1/2} = \frac{1}{2k^n}\left(g_j^n - g_{j-1}^n + g_j^{n-1} - g_{j-1}^{n-1}\right), \tag{30}$$

The finite-difference approximation of equations. (20) – (24) for the mid-point $\left(\eta_{j-1/2}, \xi^n\right)$ assume the form given below:

$$h_j^{-1}\left(f_j^n - f_{j-1}^n\right) = u_{j-1/2}^n, \tag{31}$$

$$h_j^{-1}\left(u_j^n - u_{j-1}^n\right) = v_{j-1/2}^n, \tag{32}$$

$$h_j^{-1}\left(s_j^n - s_{j-1}^n\right) = t_{j-1/2}^n, \tag{33}$$

$$\begin{aligned}&\left(v_j - v_{j-1}\right) + \left(1+\alpha+\xi\cot\xi\right)\frac{h_j}{4}\left[\left(f_j + f_{j-1}\right)\left(v_j + v_{j-1}\right)\right] - \frac{(1+\alpha)h_j}{4}\left(u_j + u_{j-1}\right)^2 + \frac{We}{2}\left(v_j + v_{j-1}\right)\left(v_j - v_{j-1}\right)\\ &- \frac{Mh_j}{2}\left(u_j + u_{j-1}\right) - \frac{\alpha h_j}{2} f_{j-1/2}^{n-1}\left(v_j + v_{j-1}\right) + \frac{Ah_j}{2}\left(s_j + s_{j-1}\right) + \frac{\alpha h_j}{2} v_{j-1/2}^{n-1}\left(f_j + f_{j-1}\right) = \left[R_1\right]_{j-1/2}^{n-1}\end{aligned} \tag{34}$$

$$\begin{aligned}&\frac{1}{\Pr}\left(t_j - t_{j-1}\right) + \left(1+\alpha+\xi\cot\xi\right)\frac{h_j}{4}\left[\left(f_j + f_{j-1}\right)\left(t_j + t_{j-1}\right)\right] - \frac{\alpha h_j}{4}\left[\left(u_j + u_{j-1}\right)\left(s_j + s_{j-1}\right)\right]\\ &+ \frac{\alpha h_j}{2} s_{j-1/2}^{n-1}\left(u_j + u_{j-1}\right) - \frac{\alpha h_j}{2} u_{j-1/2}^{n-1}\left(s_j + s_{j-1}\right) - \frac{\alpha h_j}{2} f_{j-1/2}^{n-1}\left(t_j + t_{j-1}\right) + \frac{\alpha h_j}{2} t_{j-1/2}^{n-1}\left(f_j + f_{j-1}\right) = \left[R_2\right]_{j-1/2}^{n-1}\end{aligned} \tag{35}$$

Here the following abbreviations apply:

$$\alpha = \frac{\xi^{n-1/2}}{k_n} \quad , A = \frac{\sin\left(\xi^{n-1/2}\right)}{\xi^{n-1/2}} \tag{36}$$

$$\left[R_1\right]_{j-1/2}^{n-1} = -h_j\left(\left(\frac{v_j - v_{j-1}}{h_j}\right) + +Wev_{j-1}v'_{j-1/2} + (1-\alpha)\left(u_{j-1/2}\right)^2\left(1-\alpha+\xi\cot\xi\right)\left(f_{j-1/2}v_{j-1/2}\right) + A\left(s_{j-1/2}\right) - M\left(u_{j-1/2}\right)\right) \tag{37}$$

$$\left[R_2\right]_{j-1/2}^{n-1} = -h_j\left[\frac{1}{\Pr}\left(\frac{t_j - t_{j-1}}{h_j}\right) + \alpha\left(u_{j-1/2}s_{j-1/2}\right) + \left(1-\alpha+\xi\cot\xi\right)\left(f_{j-1/2}t_{j-1/2}\right)\right] \tag{38}$$

The boundary conditions take the form:

$$f_0^n = u_0^n = 0,\ \ \theta_0^n = 1,\ \ u_J^n = 0,\ v_J^n = 0,\ \theta_J^n = 0 \tag{39}$$

The emerging non-linear system of algebraic equations is *linearized* by means of Newton's method and then solved by the *block-elimination* method. The accuracy of computations is influenced by the number of mesh points in both directions. After experimenting with various grid sizes in the η-direction (radial coordinate) a larger number of mesh points are selected whereas in the ξ direction (tangential coordinate) significantly less mesh points are utilized. η_{max} has been set at 12 and this defines a sufficiently large value at which the prescribed boundary conditions are satisfied. ξ_{max} is set at 3.0 for this flow domain. *Mesh independence* is therefore achieved in the present computations. The computer program of the algorithm is executed in MATLAB running on a PC.

4. Validation of Keller Box Solutions

The present Keller box solutions have been validated for the special case of non-magnetic (M=0) Newtonian flow (We =0) in the absence of thermal and partial slip (S_f=S_T=0). This case was considered earlier by Molla *et al*. [43]. Furthermore, when viscous dissipation and temperature-dependent properties are ignored in the model of Haque *et al.* [44] in addition to prescribing M=We=S_f=S_T=0 in the present model, it is also possible to make a comparison as the momentum equation and boundary conditions assume the following reduced form:

$$f''' + (1+\xi\cot\xi)\,ff'' - f'^2 + \frac{\sin\xi}{\xi}\theta = \xi\left(f'\frac{\partial f'}{\partial\xi} - f''\frac{\partial f}{\partial\xi}\right) \tag{40}$$

At $\eta = 0;\ \ f = 0;\ \ f' = 0,\ \ \theta = 1$

At $\eta \to \infty:\ f' \to 0;\ \ \theta \to 0$

The energy equation (15) is identical to that considered in Molla *et al.* [43] and Haque *et al.* [44]. The comparison of solutions is documented in **Table 1**. Excellent correlation is achieved and confidence in the present solutions is therefore justifiably high.

Table 1. Values of the local heat transfer coefficient $-\theta'(\xi,0)$ for various values of ξ with $We = S_f = S_T = M = 0.0$

ξ (degrees)	$\Pr = 0.7$		
	Molla *et al.*[43]	Haque *et al*. [44]	Present Solutions
0	0.4576	0.45762	0.45758
10	0.4564	0.45653	0.45690
20	0.4532	0.45336	0.45346
30	0.4479	0.44808	0.44725
40	0.4404	0.44067	0.44309
50	0.4307	0.43107	0.43277
60	0.4188	0.41920	0.41821
70	0.4045	0.40499	0.40318
80	0.3877	0.38828	0.39435
90	0.3683	0.36891	0.37247

5. Results and Discussion

Extensive computations have been conducted using the Keller box code to study the influence of the key thermo-physical parameters on velocity, temperature, skin friction and Nusselt number. These are visualized in **figs. 3a-b** to **12a-b**. In the present computations, the following default parameters are prescribed (unless otherwise stated):

$$We = 0.3, \Pr = 7.0, M = 1.0,\ S_f = 0.5,\ S_T = 1.0, \xi = 1.0$$

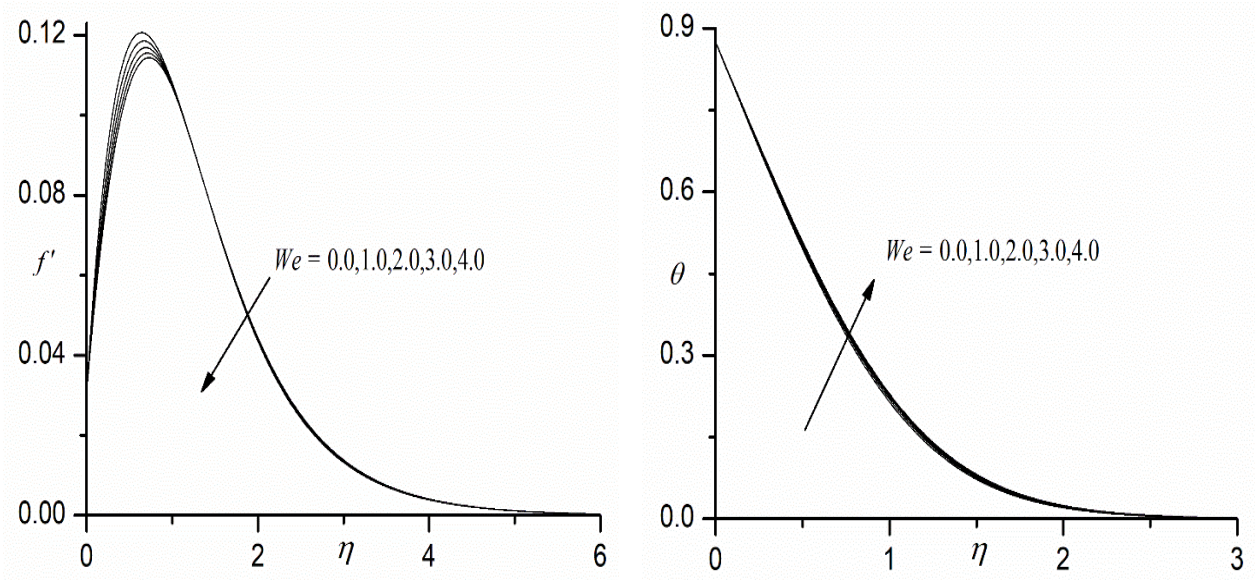

(a) (b)

Fig. 3. (a) Velocity profiles and (b) Temperature profiles for various values of *We*

Figs. 3a-b illustrate the influence of Weissenberg number (*We*) on velocity and temperature profiles. We arise only in the momentum eqn. (14) in the mixed derivative $Wef''f'''$. Weissenberg number (*We*) measures the relative effects of viscosity to elasticity. Weissenberg number is zero corresponds to a purely Newtonian fluid, and infinite Weissenberg number corresponds to a purely elastic solid. Intermediate values correlate quite well with actual polymeric viscoelastic properties. With increasing *We*, there is a general increase through the boundary layer in velocity magnitudes. The boundary layer flow is therefore accelerated as viscous effects are depleted since resistance to the flow is reduced. The momentum boundary layer is therefore depleted with greater Weissenberg number. We note that in fig. 3a the magnetic body force parameter, *M*, is set at unity implying that the Lorentzian magnetic drag and viscous hydrodynamic force are of the same magnitude. Fig. 3b shows that a consistent elevation is computed in temperature of the

viscoelastic fluid with greater values of Weissenberg number, *We*. The acceleration in the flow aids in momentum development which also assists in thermal diffusion, leading to heating of the boundary layer. Thermal boundary layer thickness is therefore *enhanced* with increasing *We* values i.e. decreasing viscosity and increasing elastic effects. Effectively therefore Newtonian fluids (We =0) achieve lower velocities and temperatures than Williamson fluids. Similar trends have been reported by Hayat *et al.* [45] and Khan and Khan [17].

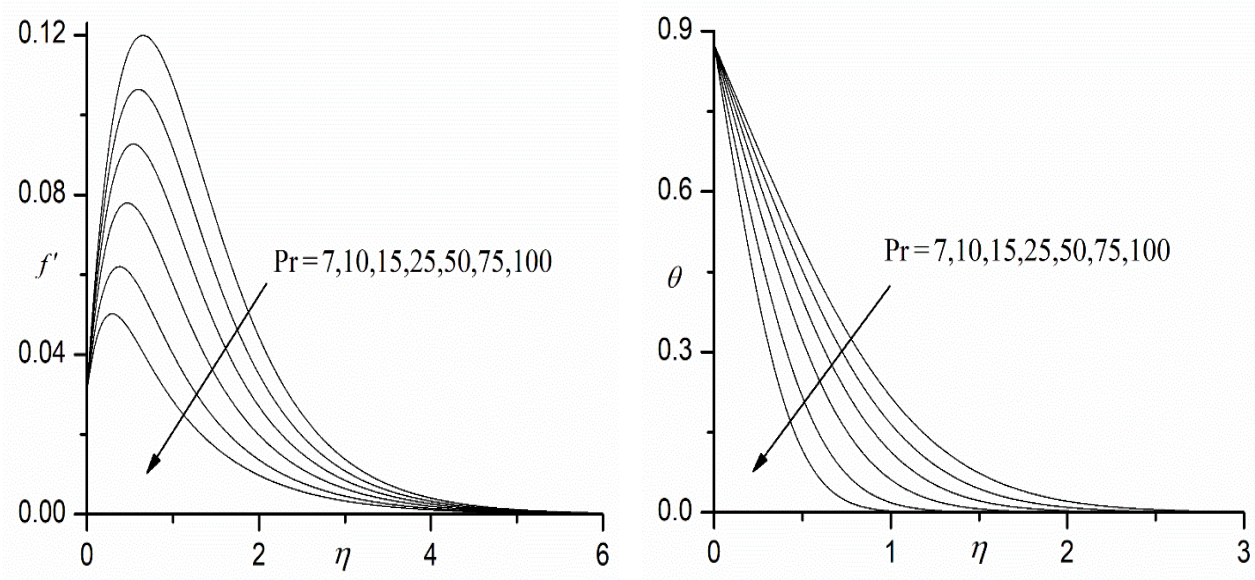

(a) (b)

Fig. 4 (a) Velocity and (b) Temperature profiles for various values of *Pr*

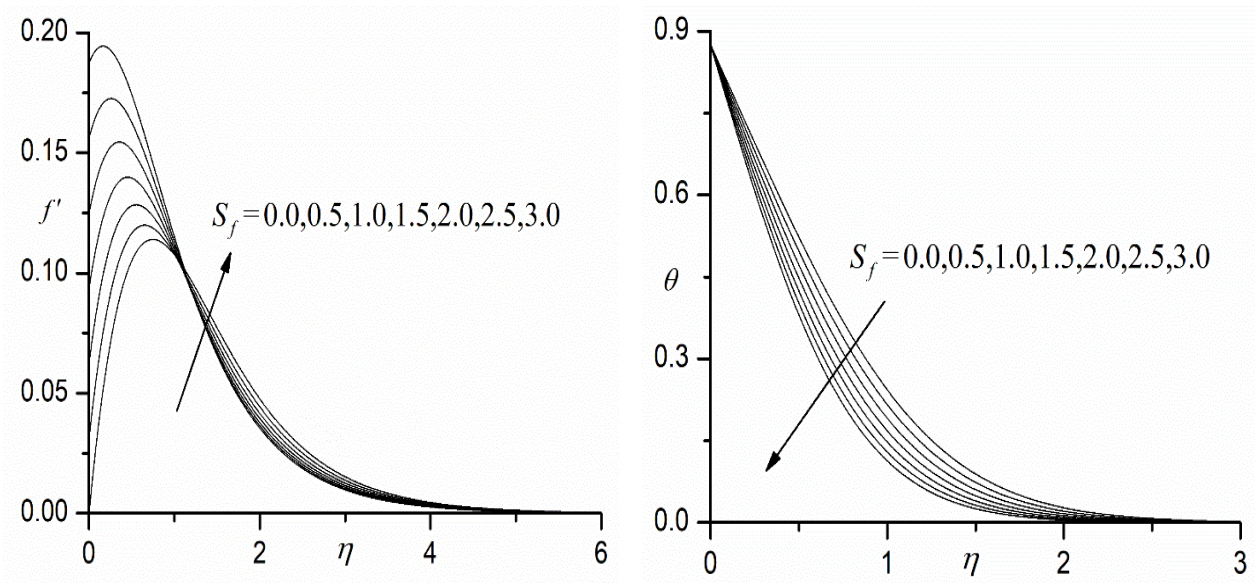

(a) (b)

Fig. 5 (a) Velocity and (b) Temperature profiles for various values of S_f

Figs. 4a-b depict the evolution in velocity and temperature characteristics with transverse coordinate i.e. normal to the sphere surface for various Prandtl numbers, *Pr*. Relatively high values of *Pr* are considered since these physically correspond to industrial polymers [46]. Prandtl number embodies the ratio of momentum diffusivity to thermal diffusivity in the boundary layer regime. It also represents the ratio of the product of specific heat capacity and dynamic viscosity, to the fluid thermal conductivity. For polymers momentum diffusion rate greatly exceeds thermal diffusion rate. The low values of thermal conductivity in most polymers also result in a high Prandtl number. With increasing *Pr* from 7 to 100 there is evidently a substantial deceleration in boundary layer flow i.e. a thickening in the momentum boundary layer (fig. 4a). The effect is most prominent close to the sphere surface. Also fig. 4b shows that with greater Prandtl number the temperature values are strongly decreased throughout the boundary layer transverse to the sphere surface. Thermal boundary layer thickness is therefore significantly reduced. The asymptotically smooth profiles in the free stream (high η values) confirm that an adequately large infinity boundary condition has been imposed in the Keller box numerical code.

Figs. 5a-b illustrate the impact of the momentum (hydrodynamic) slip parameter (S_f) on the velocity and temperature distributions. Near the sphere surface there is a distinct elevation in velocity with greater momentum slip effect. S_f features in the velocity wall boundary condition in eqn. (16) i.e. $f'(0)=S_f f''(0)$. With increasing values of S_f the polymer slips i.e. shears more easily against the sphere surface. This boosts momentum in the boundary layer and accelerates the flow (fig. 5a). However, with progressive penetration into the boundary layer, this effect is reversed (as expected) and the flow is decelerated with greater momentum slip further from the sphere surface. The velocity slip effect is strongest at the sphere surface (η = 0). A similar observation has been made by Yarin and Graham [25] and also by Jamil and Khan [34]. The momentum slip effect is prominent and substantially modifies the velocity growth structure. Temperature is conversely reduced consistently throughout the boundary layer with greater momentum slip. The viscoelastic polymer is therefore cooled with wall momentum slip and this reduces thermal boundary layer thickness. The implication is therefore that with an absence of velocity slip in mathematical models, temperature is over-predicted (the maximum value corresponds to S_f =0). It is therefore important in more realistic simulations of polymer coating dynamics to incorporate wall slip effects.

Figs. 6a-b present the response in velocity and temperature distributions to a modification in the thermal jump (slip) parameter (S_T). A marked depletion in velocity (fig. 6a) accompanies an increase in thermal slip effect and this trend is sustained throughout the boundary layer. The thermal slip parameter indirectly influences the momentum field via coupling to the energy

equation (thermal slip is only simulated in the wall thermal boundary condition in eqn. 16). With greater thermal slip, there is also a very profound depletion in temperature at the sphere surface and in close proximity to it (fig. 6b). However, this effect weakens considerably with further distance from the sphere surface and is effectively eliminated before reaching the free stream. Temperature profiles decay from a maximum at the sphere surface to the free stream. All profiles converge at a large value of transverse coordinate, again showing that a sufficiently large infinity boundary condition has been utilized in the numerical computations. Again the absence of thermal slip achieves higher temperatures indicating that without this modification in the thermal boundary condition at the wall (sphere surface) the temperature is over-predicted, which can be critical to heat treatment of polymeric coatings [47].

Figs. 7a-b present the evolution in velocity and temperature functions with a variation in magnetic body force parameter (*M*). The radial magnetic field generates a transverse retarding body force. This decelerates the boundary layer flow and velocities are therefore reduced as observed in fig. 7a. The momentum development in the viscoelastic coating can therefore be controlled using a radial magnetic field. The effect is prominent throughout the boundary layer from the sphere surface to the free stream. Momentum (hydrodynamic) boundary layer thickness is therefore increased with greater magnetic field. Fig. 7b shows that the temperature is strongly enhanced with greater magnetic parameter. The excess work expended in dragging the polymer against the action of the magnetic field is dissipated as thermal energy (heat). This energizes the boundary layer and increases thermal boundary layer thickness. Again the influence of magnetic field is sustained throughout the entire boundary layer domain. These results concur with other investigations of magnetic non-Newtonian heat transfer including Kasim *et al*. [24].

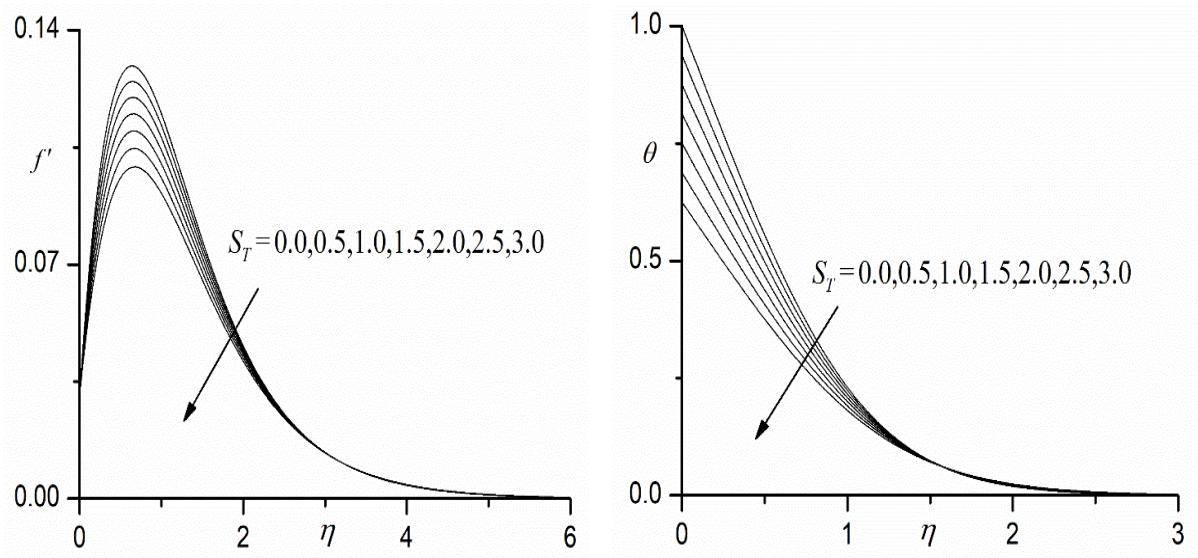

(a) (b)

Fig. 6 (a) Velocity and (b) Temperature profiles for various values of S_T

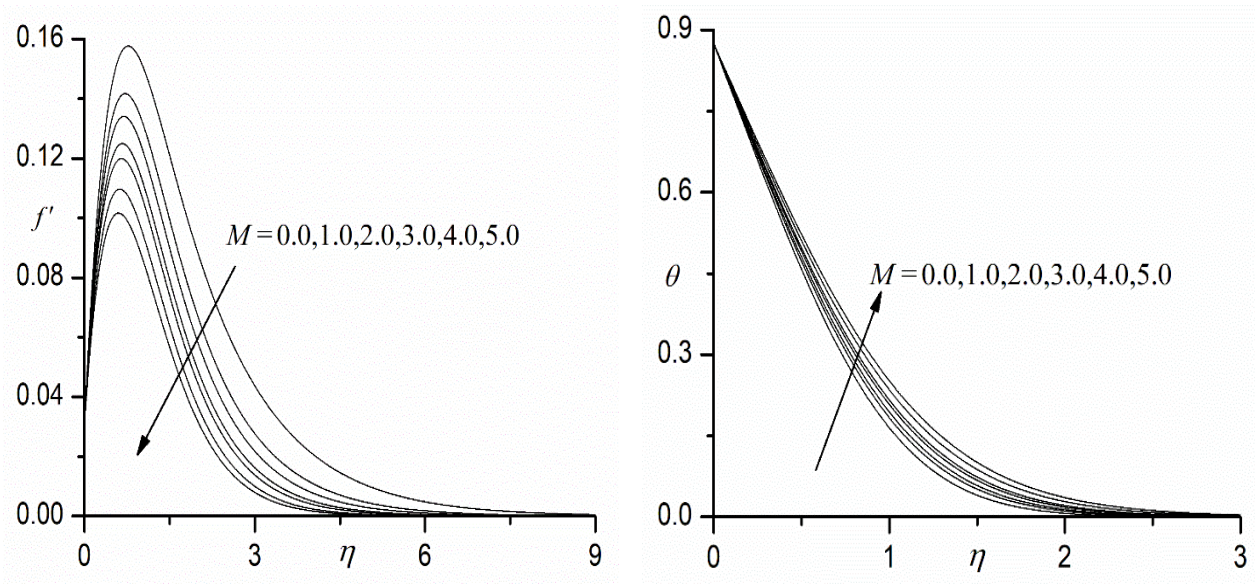

(a) (b)

Fig. 7 (a) Velocity and (b) Temperature profiles for various values of M

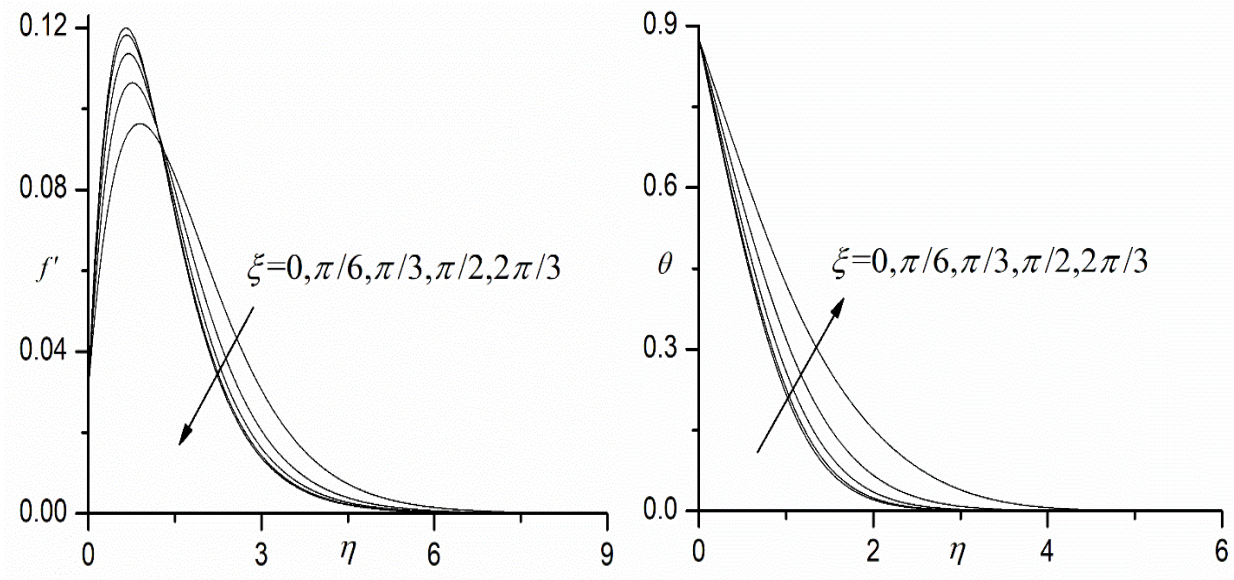

(a) (b)

Fig. 8 (a) Velocity and (b) Temperature profiles for various values of ξ

Figs. 8a-b illustrate the influence of the stream wise (tangential) coordinate, ξ, on the velocity and temperature distributions. A weak deceleration in the boundary layer flow is experienced with greater ξ, values i.e. with progressive distance along the sphere surface from the lower stagnation point ($\xi=0$), as shown in fig. 8a. Momentum boundary layer thickness is therefore increased marginally with ξ values. Conversely a weak enhancement in temperature is

computed in fig. 8b, with increasing ξ values. Thermal boundary layer thickness is increased therefore as we progress from the lower stagnation point on the sphere surface around the sphere periphery upwards.

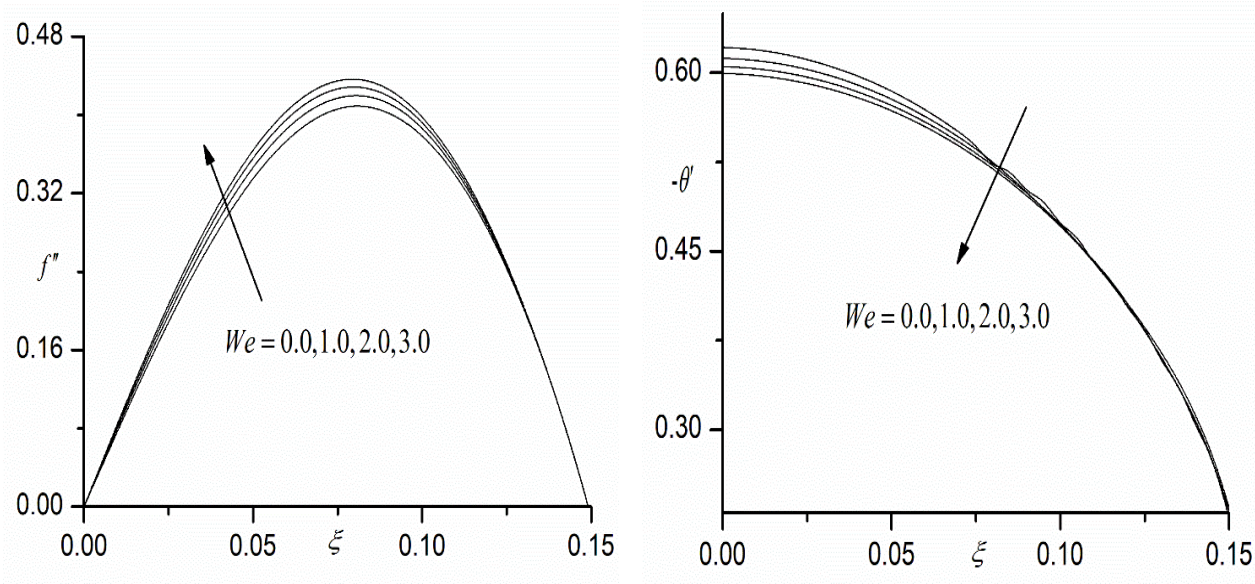

(a) (b)

Fig. 9 (a) Skin friction and b. Nusselt number profiles for various values of *We*

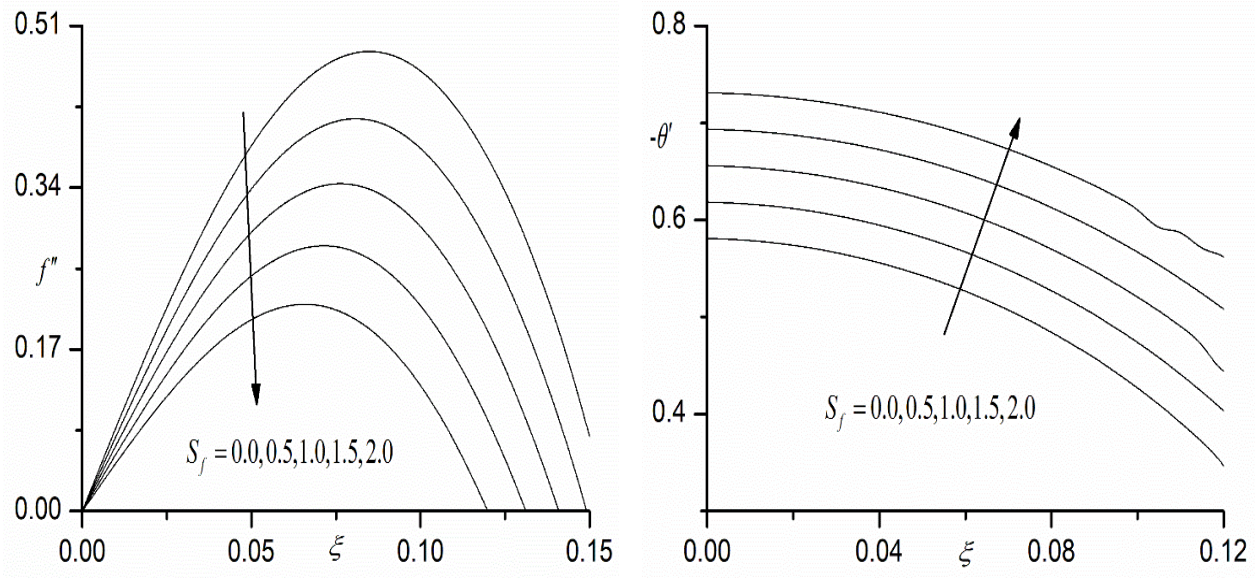

(a) (b)

Fig. 10 (a) Skin friction and (b) Nusselt number profiles for various values of S_f

Figs. 9a-b presents the variation in surface shear stress (skin friction) and Nusselt number (wall heat transfer gradient) with Weissenberg number with both thermal and velocity slip

present. In consistency with the near-wall behaviour computed for the velocity field in fig. 3a, there is a significant elevation in skin friction with increasing *We* values. With progressively greater *We* values the elasticity in the polymer is increased. This aids in momentum development and accelerates the boundary layer flow. A similar trend has been computed in the studies by Hayat *et al*. [45]. The Weissenberg number indicates the degree of anisotropy or orientation generated by the deformation, and is appropriate to describe flows with a constant stretch history, and therefore appropriate for polymers. A strong reduction in Nusselt number arises with an elevation in Weissenberg number i.e. heat is transferred from the sphere surface to the boundary layer. This concurs with fig. 3b wherein temperature (and thermal boundary layer thickness) are found to be enhanced with Wiessenberg number. The sphere surface is therefore effectively cooled with greater Weissenberg numbers.

Figs. 10a-b illustrate the skin friction and Nusselt number distributions with various values of momentum slip parameter (S_f). A marked depreciation in skin friction is observed with greater momentum slip (fig. 10a). Conversely a strong elevation in Nusselt number is generated with greater momentum slip effect (fig. 10b). In both plots the profiles never intersect i.e. the momentum slip effect is consistent for all values of stream wise parameter (ξ). The influence of momentum (hydrodynamic) slip is non-trivial and demonstrates that a sizeable modification in surface thermo-fluid characteristics is induced with slip and indeed that the methodology employed to simulate it quite realistically simulates real macroscopic effects of certain molecular phenomena at polymer/solid interfaces.

Table 2. Values of $f''(\xi,0)$ and $-\theta'(\xi,0)$ for different S_f, S_T and ξ

S_f	S_T	$f''(\xi,0)$			$-\theta'(\xi,0)$		
		$\xi=0.0$	$\xi=\pi/6$	$\xi=\pi/4$	$\xi=0.0$	$\xi=\pi/6$	$\xi=\pi/4$
0.0	1.0	0	0.1908	0.2592	0.7199	0.7015	0.6857
0.1		0	0.1858	0.2522	0.7326	0.7140	0.6981
0.2		0	0.1807	0.2453	0.7454	0.7266	0.7105
0.3		0	0.1757	0.2383	0.7582	0.7393	0.7229
0.5		0	0.1657	0.2244	0.7839	0.7645	0.7475
0.8		0	0.1506	0.2036	0.8225	0.8026	0.7850
1.0		0	0.1406	0.1897	0.8483	0.8279	0.8100
0.5	0.0	0	0.1871	0.2536	0.9259	0.9032	0.8835
	0.5	0	0.1765	0.2391	0.8543	0.8333	0.8151

	1.5	0	0.1547	0.2096	0.7147	0.6979	0.6814
	2.0	0	0.1437	0.1945	0.6469	0.6308	0.6166
	2.5	0	0.1324	0.1792	0.5804	0.5659	0.5532
	3.0	0	0.1210	0.1636	0.5154	0.5025	0.4911

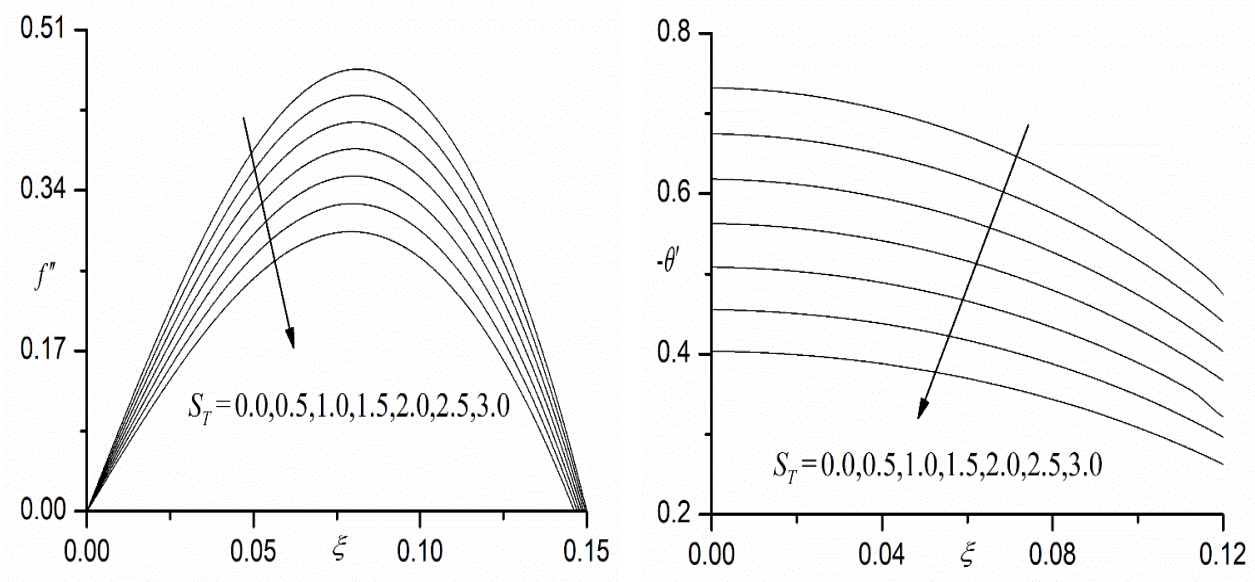

(a) (b)

Fig. 11 (a) Skin friction and (b) Nusselt number profiles for various values of S_T

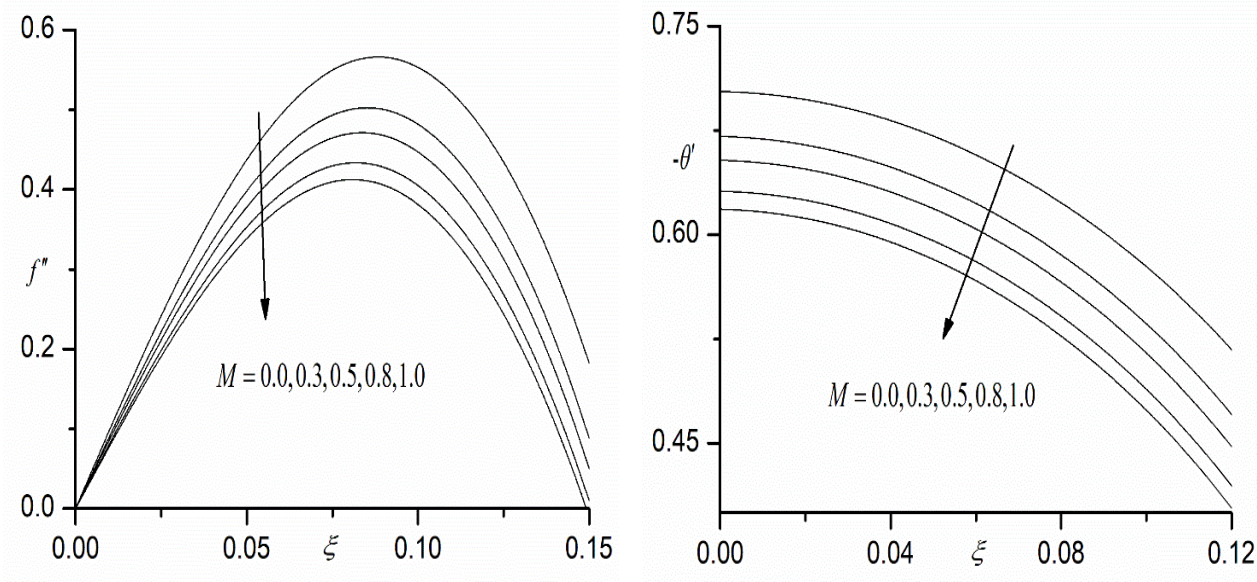

(a) (b)

Fig. 12 (a) Skin friction and (b) Nusselt number profiles for various values of M

Figs. 11a-b present the distributions in skin friction and Nusselt number with thermal slip effect (S_T). Both skin friction and Nusselt number are strongly reduced with an increase thermal

slip. The boundary layer is therefore decelerated and heated with stronger thermal slip. With thermal slip absent therefore the skin friction is maximized at the sphere surface. The inclusion of thermal slip, which is encountered in various slippy polymer flows, is therefore important in more physically realistic simulations.

Figs. 12a-b illustrate the influence of magnetic parameter (*M*) on skin friction and Nusselt number. A significant depletion is caused in skin friction (fig. 12a) with greater magnetic field, which corresponds to a retardation of the boundary layer flow. The maximum skin friction therefore is achieved only in the absence of a radial magnetic field i.e. $M = 0$. For $M < 1$, the magnetic body force is exceeded by the viscous hydrodynamic force in the regime. For $M > 1$ the contrary is the case. The reduction in Nusselt number with greater *M* values implies that the transfer of heat from the boundary layer to the wall (sphere surface) is reduced. This physically indicates therefore that greater heat is conveyed away from the sphere surface to the fluid which explains the higher temperatures associated with strong magnetic field in the earlier computations (fig. 7b). Magnetic field is therefore a potent mechanism for controlling thermal and velocity characteristics in electrically-conducting polymer dynamics.

Table 3. Values of $f''(\xi,0)$ and $-\theta'(\xi,0)$ for different S_f, S_T and ξ

S_f	S_T	$f''(\xi,0)$			$-\theta'(\xi,0)$		
		$\xi=\pi/3$	$\xi=\pi/2$	$\xi=2\pi/3$	$\xi=\pi/3$	$\xi=\pi/2$	$\xi=2\pi/3$
0.0	1.0	0.3473	0.4415	0.4506	0.6521	0.5687	0.4466
0.1		0.3376	0.4280	0.4344	0.6641	0.5795	0.4554
0.2		0.3280	0.4144	0.4182	0.6761	0.5904	0.4638
0.3		0.3183	0.4009	0.4020	0.6883	0.6013	0.4727
0.5		0.2989	0.3738	0.3694	0.7125	0.6234	0.4904
0.8		0.2699	0.3330	0.3204	0.7492	0.6563	0.5173
1.0		0.2504	0.3058	0.2876	0.7726	0.6786	0.5351
0.5	0.0	0.3382	0.4241	0.4218	0.8421	0.7374	0.5814
	0.5	0.3187	0.3991	0.3957	0.7767	0.6798	0.5355
	1.5	0.2790	0.3481	0.3427	0.6494	0.5678	0.4462
	2.0	0.2587	0.3222	0.3157	0.5875	0.5134	0.4029
	2.5	0.2381	0.2958	0.2884	0.5272	0.4601	0.3607
	3.0	0.2172	0.2690	0.2606	0.4680	0.4080	0.3194

Table 4. Values of $f''(\xi,0)$ and $-\theta'(\xi,0)$ for different values of We, M and Pr									
We	M	$f''(\xi,0)$				$-\theta'(\xi,0)$			
		$\Pr = 7$	$\Pr = 10$	$\Pr = 20$	$\Pr = 25$	$\Pr = 7$	$\Pr = 10$	$\Pr = 20$	$\Pr = 25$
0.0	1.0	0.2960	0.2730	0.2294	0.2157	0.7145	0.8098	1.0370	1.1239
0.5		0.3008	0.2769	0.2316	0.2176	0.7104	0.8063	1.0322	1.1190
1.0		0.3049	0.2803	0.2341	0.2198	0.7072	0.8028	1.0289	1.1158
2.0		0.3122	0.2864	0.2382	0.2234	0.7012	0.7966	1.0226	1.1095
3.0		0.3185	0.2916	0.2417	0.2265	0.6961	0.7912	1.0168	1.1036
4.0		0.3240	0.2964	0.2449	0.2294	0.6917	0.7865	1.0117	1.0986
0.3	0.0	0.3760	0.3444	0.2870	0.2698	0.8013	0.9019	1.1364	1.2267
	0.5	0.3302	0.3029	0.2529	0.2376	0.7497	0.8463	1.0747	1.1628
	1.0	0.2989	0.2753	0.2308	0.2170	0.7125	0.8089	1.0330	1.1213
	2.0	0.2538	0.2352	0.1988	0.1872	0.6568	0.7512	0.9736	1.0593
	3.0	0.2203	0.2052	0.1745	0.1645	0.6144	0.7072	0.9277	1.0122
	4.0	0.1936	0.1809	0.1546	0.1457	0.5799	0.6710	0.8902	0.9735

Tables 2-5 present numerical values for the influence of the various parameters on skin friction and Nusselt number functions. These confirm the trends already elaborated in figs 9a-b to 12a-b and furthermore provide benchmarks against which other researchers may validate extensions of the present model.

Table 5: Values of $f''(\xi,0)$ and $-\theta'(\xi,0)$ for different values of We, M and Pr							
We	M	$f''(\xi,0)$			$-\theta'(\xi,0)$		
		$\Pr = 50$	$\Pr = 75$	$\Pr = 100$	$\Pr = 50$	$\Pr = 75$	$\Pr = 100$
0.0	1.0	0.1749	0.1524	0.1370	1.4513	1.6946	1.8975
0.5		0.1762	0.1533	0.1377	1.4473	1.6911	1.8942
1.0		0.1771	0.1541	0.1383	1.4430	1.6879	1.8913
2.0		0.1795	0.1557	0.1393	1.4376	1.6821	1.8846
3.0		0.1815	0.1571	0.1407	1.4321	1.6769	1.8812
4.0		0.1833	0.1584	0.1417	1.4272	1.6724	1.8770
0.3	0.0	0.2194	0.1924	0.1745	1.5630	1.8118	2.0183
	0.5	0.1923	0.1677	0.1512	1.4925	1.7373	1.9413

	1.0	0.1757	0.1529	0.1374	1.4489	1.6925	1.8955
	2.0	0.1517	0.1315	0.1175	1.3850	1.6270	1.8289
	3.0	0.1332	0.1149	0.1022	1.3355	1.5762	1.7772
	4.0	0.1177	0.1011	0.0893	1.2928	1.5333	1.7334

5. Conclusion

Motivated by applications in thermal processing of magnetic polymers in coating systems, a mathematical model has been developed for the Magnetohydrodynamic flow and heat transfer in an electro-conductive viscoelastic Williamson fluid from a spherical body under radial magnetic field. To simulate slippery polymer interfacial effects, both thermal and momentum slip have been incorporated into the model. The normalized, nonlinear two-dimensional, steady state boundary layer equations for momentum and heat (energy) have been solved with a finite difference scheme, with verification of computational accuracy demonstrated via benchmarking with earlier non-magnetic, no slip, Newtonian solutions in the literature. The present computations have shown that increasing Weissenberg number accelerates the near-wall flow and also increases temperatures (i.e reduces Nusselt number). Stronger magnetic parameter serves to decelerate the flow and to elevate temperatures i.e. decreases Nusselt numbers. With greater momentum slip the flow is accelerated near the sphere surface whereas temperatures are depressed i.e. Nusselt numbers are increased. With greater thermal slip surface skin friction and Nusselt number are both significantly suppressed.

Acknowledgement

The authors appreciate the constructive comments of the reviewers which led to definite improvement in the paper. The authors are thankful to the Management of Madanapalle Institute of Technology & Science, Madanapalle for providing research facilities in the campus.

References

1. J.A. Rojas, K. Santos, Magnetic nanophases of iron oxide embedded in polymer. Effects of magneto-hydrodynamic treatment of pure and wastewater, 2011, 5th Latin American Congress on Biomedical Engineering CLAIB 2011 May 16-21. Habana, Cuba.
2. H. Yonemura, M. Takata, S. Yamada, Magnetic field effects on photo electrochemical reactions of electrodes modified with thin films consisting of conductive polymers, 2014, J. Appl. Phys., vol. 53.

3. G.V. Stepanov, S.S. Abramchuk, D.A. Grishin, L.V. Nikitin, EYu. Kramarenko, A.R. Khokhlov, Effect of a homogenous magnetic field on the viscoelastic behavior of magnetic elastomers, 2007, Polymer, vol. 48. pp. 488–495.
4. X.U. Zengyu et al., MHD effects caused by insulator coating imperfections, 1998, Fusion Engin. Design, vol. 40, pp. 739- 798. http://dx.doi.org/10.1016/S0920-3796(98)00303-2.
5. Liu Zhaohui, Yidong Ding, Xin Shu, Na Liu, Preparation, Characterization and Properties of SiO2 Aerogel Composite Thermal Insulation Coating, 2016, Chemical Engineering Transactions, vol. 55, 259-264.
6. H. Yamaguchi, X.R. Zhang, S. Higashi, M. Li, Study on power generation using electro-conductive polymer and its mixture with magnetic fluid, 2007, J. Magnetism and Magnetic Materials, vol. 320, no. 7, pp. 1406–1411. http://dx.doi.org/10.1016/j.jmmm.2007.12.014
7. T.A. Bég, O.A. Bég, M.M. Rashidi, M. Asadi, Homotopy semi-numerical modelling of nanofluid convection flow from an isothermal spherical body in a permeable regime, 2012, Int. J. Microscale Nanoscale Therm. Fluid Transp. Phenom., vol. 3, pp. 237–66.
8. S.G. Musong, Z.G.Feng, Mixed convective heat transfer from a heated sphere at an arbitrary incident flow angle in laminar flows, 2014, Int. J. Heat and Mass Transfer, vol. 78, pp. 34-44.
9. G. Juncu, The influence of viscous dissipation on the unsteady conjugate forced convection heat transfer from a fluid sphere, 2015, Int. J. Heat and Mass Transfer, vol. 90, pp. 542-551.
10. R.L. Verma, Elastico-viscous boundary-layer flow on the surface of sphere, 1977, Rhelogica Acta, vol. 16, pp. 510-515.
11. C.Y. Cheng, Natural convection heat and mass transfer from a sphere in micropolar fluids with constant wall temperature and concentration, 2008, Int. Commun. Heat Mass Transf., vol. 35, pp. 750–75.
12. C.H. Amanulla, N. Nagendra, M. Suryanarayana Reddy, A. Subba Rao, O.A. Bég, Mathematical Study of Non-Newtonian Nanofluid Transport Phenomena from an Isothermal Sphere, 2017, Frontiers in Heat and Mass Transfer, vol. 8, 29. http://dx.doi.org/10.5098/hmt.8.29
13. A. Dasman, A.R.M. Kasim, N.F. Mohammad, A. Mangi, S. Shafie, Mixed convection boundary layer flow of viscoelastic fluids past a sphere, 2013, Defect and Diffusion Forum, vol. 336, pp. 57-63.
14. A. Dasman, Mixed convection boundary layer flow of a viscoelastic fluid past a sphere, 2010, Masters thesis, Universiti Teknologi Malaysia, Faculty of Science.
15. R.K. Bhatnagar, On heat transfer in a viscoelastic fluid flowing around a steadily rotating and thermally insulated sphere, 1970, Rheologica Acta, vol. 9, pp. 419–423.

16. F. Mabood, S. M. Ibrahim, G. Lorenzini, and E. Lorenzini, Raduation effects on Williamson nanofluid over a heated surface with Magnetohydrodynamics, 2017, Int. J. Heat. Tech. vol. 35, no. 1, pp. 196-204.
17. N.A. Khan, H. Khan, A Boundary layer flows of non-Newtonian Williamson fluid, 2014, Nonlinear Eng., vol. 3, no. 2, pp. 107–115. http://dx.doi.org/10.1515/nleng-2014-0002.
18. O.A. Bég, M. Keimanesh, M.M. Rashidi, M. Davoodi, Multi-step DTM simulation of magneto-peristaltic flow of a conducting Williamson viscoelastic fluid, 2013, Int. J. Appl. Math. Mech., vol. 9, no. 6, pp. 1-19.
19. K.S. Rao, P.K. Rao, Fully developed free convective flow of a Williamson fluid through a porous medium in a vertical channel, 2014, Int. J. Conceptions on Computing and Information Technology, vol. 2, pp. 54-57.
20. I. Dapra, G. Scarpi, Perturbation solution for pulsatile flow of a non-Newtonian Williamson fluid in a rock fracture, 2007, Int. J. Rock Mech., Mining Sci., vol. 44, pp. 271–278.
21. O.A. Bég, J. Zueco, M. Norouzi, M. Davoodi, A.A. Joneidi, A.F. Elsayed, Network and Nakamura tridiagonal computational simulation of electrically-conducting biopolymer micro-morphic transport phenomena, 2014, Comp. Biology and Medicine, vol. 44, pp. 44–56.
22. H.T. Alkasasbeh, M.Z. Salleh, R. Naza, I. Pop, Numerical solutions of radiation effect on Magnetohydrodynamic free convection boundary layer flow about a solid sphere with Newtonian heating, 2014, Applied Mathematical Sciences, vol. 8, pp. 6989 – 7000.
23. C.H. Amanulla, N. Nagendra, M. Surya Narayana Reddy, Numerical Study of Thermal and Momentum Slip Effects on MHD Williamson Nanofluid from an Isothermal Sphere, 2017, Journal of Nanofluids, vol. 6, no. 6, pp. 1111–1126. https://doi.org/10.1166/jon.2017.1405
24. A.R.M. Kasim, N.F. Mohammad, I. Anwar, S. Shafie, MHD effect on convective boundary layer flow of a viscoelastic fluid embedded in porous medium with Newtonian heating, 2013, Recent Advances in Mathematics, vol. 4, pp. 182-189.
25. A.L. Yarin, M.D. Graham, A model for slip at polymer/solid interfaces, 1998, J. Rheol., vol. 42, no. 6, pp. 1491–1504.
26. J.M. Piau, N.E. Kissi, Measurement and modelling of friction in polymer melts during macroscopic slip at the wall, 1994, J. Non-Newtonian Fluid Mech., vol. 54, pp. 121–142.
27. J.M. Piau, N.E. Kissi, F. Toussaint, A. Mezghani, Distortions of polymer extrudates and their elimination using slippery surfaces, 1995, Rheol. Acta, vol. 34, pp. 40–57.
28. F.J. Lim, W.R. Schowalter, Wall slip of narrow molecular weight distribution polybutadienes, 1989, J. Rheol., vol. 33, no.8, pp. 1359–1382.

29. K.B. Migler, H. Hervet, L. Leger, Slip transition of a polymer melt under shear stress, 1993, Physical Review Letters, vol. 70, pp. 287–290.
30. S.G. Hatzikiriakos, J.M. Dealy, Wall slip of molten high density polyethylenes. II. Capillary rheometer studies, 1992, J. Rheology, vol. 36, pp. 703–741.
31. W.B. Blac, Wall slip and boundary effects in polymer shear flows, 2000, PhD Thesis, Chemical Engineering, University of Wisconsin – Madison, USA.
32. S.G. Hatzikiriakos, J.M. Dealy, Wall slip of molten high density polyethylene. I. Sliding plate rheometer studies, 1991, *J. Rheol*., vol. 35, no.4, pp. 497–523.
33. F. Brochard, P.G.D. Gennes, Shear-dependent slippage at a polymer/solid interface, 1992, Langmuir, vol. 8, no. 12, pp. 3033–3037.http://dx.doi.org/10.1021/la00048a030.
34. M. Jamil, N.A. Khan, Slip effects on fractional viscoelastic fluids, 2011, Int. J. Differential Equations, vol. 2011, no. 2011, pp. 1-19.http://dx.doi.org/10.1155/2011/193813.
35. D. Tripathi, O.A. Bég, J.L. Curiel-Sosa, Peristaltic flow of generalized Oldroyd- B fluids with slip effects, 2014, Comp. Methods in Biomechanics Biomedical Eng., Vol. 17, pp. 433-442.
36. O.A. Bég, M.J. Uddin, M.M. Rashidi, N. Kavyani, Double-diffusive radiative magnetic mixed convective slip flow with Biot and Richardson number effects, 2014, J. Engineering Thermophysics, vol. 23, no. 2, pp. 79–97.
37. S.P.A. Devi, R.U. Devi, Soret and Dufour effects on MHD slip flow with thermal radiation over a porous rotating infinite disk, 2011, Comm. Nonlinear Science and Numerical Simulation, vol. 16, no. 4, pp. 1917–1930. http://dx.doi.org/10.1016/j.cnsns.2010.08.020.
38. C.H. Amanulla, N. Nagendra, M. Suryanarayana Reddy, Thermal and Momentum Slip Effects on Hydromagnetic Convection Flow of a Williamson Fluid Past a Vertical Truncated Cone, 2017, Frontiers in Heat and Mass Transfer, vol. 9, 22. http://dx.doi.org/10.5098/hmt.9.22
39. H.B. Keller, Numerical Solution of Two-Point Boundary Value Problems, 1976, SIAM Press, Philadelphia, USA.
40. M. Sajid, S.A. Iqbal, M. Naveed, Z. Abbas, Joule heating and Magnetohydrodynamic effects on ferrofluid (Fe3O4) flow in a semi-porous curved channel, 2016, J. Molecular Liquids, vol. 222, pp. 1115-1120.http://dx.doi.org/10.1016/j.molliq.2016.08.001.
41. C.H. Amanulla, N. Nagendra, M. Suryanarayana Reddy, MHD Flow and Heat Transfer in a Williamson Fluid from a Vertical Permeable Cone with Thermal and Momentum Slip Effects: A Mathematical Study, 2017, Frontiers in Heat and Mass Transfer, vol. 8, 40. http://dx.doi.org/10.5098/hmt.8.40.

42. C.H. Amanulla, N. Nagendra, A. Subba Rao, O.A. Bég, A. Kadir, Numerical exploration of thermal radiation and Biot number effects on the flow of a non-Newtonian MHD Williamson fluid over a vertical convective surface, 2017, Heat Trans Asian Res. 2017;00:1–19. https://doi.org/10.1002/htj.21303
43. M.M. Molla, M.A. Taher, M.M.K. Chowdhury, M.A. Hossain, Magnetohydrodynamic natural convection flow on a sphere in presence of heat generation, 2005, Nonlinear Analysis Modelling and Control, Vol. 10, pp. 349-363.
44. M.R. Haque, M.M. Alam, M.M. Ali, R. Karim, Effects of viscous dissipation on natural convection flow over a sphere with temperature dependent thermal conductivity in the presence of heat generation, 2015, Procedia Engineering, vol. 105, pp. 215-224.
45. T. Hayat, A. Shafiq, A. Alsaedi, Hydromagnetic boundary layer flow of Williamson fluid in the presence of thermal radiation and Ohmic dissipation, 2016, Alexandria Engineering Journal., vol. 55, no. 3, pp. 2229–2240. http://dx.doi.org/10.1016/j.aej.2016.06.004.
46. S. Sato, K. Oka, A. Murakami, Heat transfer behavior of melting polymers in laminar flow field, 2004, Polymer Engineering and Science, Vol. 44, pp. 423-432. http://dx.doi.org/10.1002/pen.20038.
47. A.A. Aly, Heat treatment of polymers: a review, 2015, Int. J. Materials Chemistry and Physics, Vol. 1, no. 2, pp. 132-140.

Nomenclature

a	radius of the sphere
B_0	externally imposed radial magnetic field
Cf	skin friction coefficient
f	non-dimensional stream function
g	acceleration due to gravity
Gr	Grashof (free convection) number
K_0	thermal jump factor
N_0	velocity (momentum) slip factor
M	magnetic body force parameter
r(x)	radial distance from symmetrical axis to surface of the sphere surface of the sphere
S_f	non-dimensional velocity slip parameter
S_T	non-dimensional thermal jump parameter
Nu	local Nusselt number

We	Weissenberg (viscoelasticity) number
T	temperature
u, v	non-dimensional velocity components along the x- and y- directions, respectively
x	stream wise coordinate
y	transverse coordinate

Greek symbols

α	thermal diffusivity
β	coefficient of thermal expansion
η	dimensionless transverse coordinate
ν	kinematic viscosity
θ	non-dimensional temperature
ρ	density of viscoelastic fluid
σ	electrical conductivity of viscoelastic fluid
Γ	time-dependent material constant
ξ	dimensionless steam wise coordinate
ψ	dimensionless stream function

Subscripts

W	conditions on the wall
∞	Free stream conditions